JOURNAL OF MATERIALS SCIENCE 20 (1985) 3668–3674

On the toughness of particulate filled polymers

A. G. EVANS
Department of Materials Science and Mineral Engineering, University of California, Berkeley, California, USA

S. WILLIAMS, P. W. R. BEAUMONT
Engineering Department, Cambridge University, Cambridge, UK

An approach for predicting trends in the toughness of particulate filled polymers has been presented. The approach is based on independent knowledge of the constitutive law that describes the non-linear behaviour in the process zone. An idealized law is used to demonstrate expected trends with particulate volume fraction and size. The trends are correlated with experimental data. Some discussion of the non-linear process zone mechanisms, such as debonding and microcracking, is presented as a basis for developing more realistic constitutive laws and hence, providing superior predictions of toughness.

1. Introduction

The toughness of polymeric solids can be enhanced by the incorporation of glass, or other hard second phases [1–3]. The toughening has been attributed to a number of different mechanisms, such as crack bowing, debonding and microcracking. The present article attempts an interpretation predicated on the recent observation [3] that substantial debonding of the second phase occurs around the crack tip and hence, that the toughening relates in some manner to the extent of debonding.

Debonding results in a non-linear stress–strain curve and a reduced secant modulus [3, 4] as depicted in Fig. 1. Representation of this deformation behaviour by a constitutive law allows computation of the toughness, without detailed knowledge of the associated microstructural processes [5, 6]. Specifically, during initial propagation of a sharp precrack, a frontal process zone develops as the load is applied and material elements within the process zone experience monotonic straining (Fig. 2). For this condition, J is generally path independent [5] and thus, J_∞, determined on a contour remote from the crack tip (in the elastic zone for small scale yielding) and J_t for a contour in the immediate vicinity of the crack tip (Fig. 2) are equal:

$$J_\infty = J_t \tag{1}$$

The stress intensity factors, K_∞^2 and K_t^2, are thus related by:

$$K_\infty^2/E = K_t^2/E_T \tag{2}$$

where E is Young's modulus and E_T is the tangent modulus of material elements at the crack tip. Consequently, since $E_T < E$ (Fig. 1), $K_t < K_\infty$, and hence, the crack tip stresses are reduced in the presence of the debond process zone. However, the reduced stress does not necessarily coincide with an enhanced toughness, because the debonding process *degrades* the material in the process zone ahead of the crack [6]. Countervailing influences thus operate within a frontal process zone.

Propagation of the crack into the debond zone results in a process zone wake (Fig. 3), because the stress–strain relation is non-reversible (Fig. 1). In the presence of a *steady-state wake* (Fig. 3), the energy density associated with a contour passing through the wake differs from that for a crack tip contour, such that [5]:

$$J_\infty = J_t + 2\int_0^h U(y)\,dy \tag{3}$$

where h is the width of the debond zone (Fig. 3)

0022–2461/85 $03.00 + .12

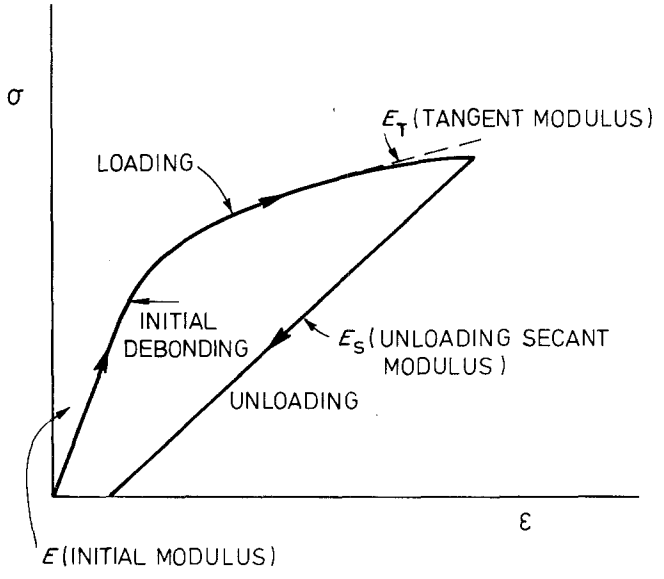

Figure 1 A non-linear stress–strain curve typical of a particulate filled polymer.

and $U(y)$ is the residual energy density in a strip dy in the remote wake. The energy density $U(y)$ is simply the area under the stress–strain curve given in Fig. 1. The change in J induced by the wake is, in fact, a direct measure of the hysteresis in the stress–strain curve, because material elements that traverse from the front of the crack to the remote wake (i.e. the energy change brought about by crack advance) are exposed to a complete stress–strain cycle (Fig. 3).

Computations of the stress–strain hysteresis in the debond process zone can be used to predict the change in J_t. The increase in toughness can then be determined by equating J_t to the local crack propagation resistance of the debonded material. The computations are strictly valid when the components of the stress tensor are consistent with a path independent J for the frontal zone. Such conditions are assumed to be approximately valid for the polymer systems of present interest.

The analysis presented in this article is based on the stress–strain characteristics of the material, as outlined above. However, some consideration is first given to the debonding and deformation mechanisms that determine the observed stress–strain relations.

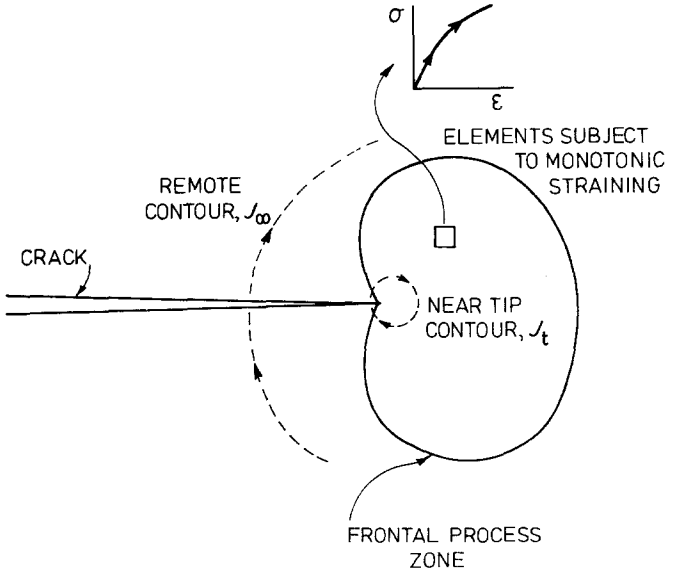

Figure 2 A frontal process zone with an associated stress–strain curve for elements within the zone; also shown are two J contours.

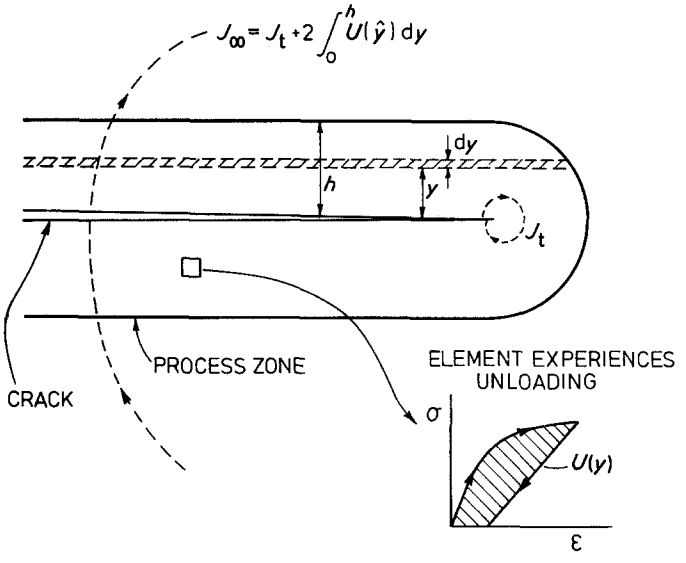

Figure 3 An extended zone indicating the hysteresis in the stress–strain curve for material elements in the wake.

2. Non-linear stress–strain relations for filled polymers

Recent studies have revealed that the onset of non-linearity in the stress–strain curve for filled polymers coincides with the debonding of the second phase [3, 4]. Debonding presumably occurs when the applied strain at the interface overcomes both the initial thermal contraction mismatch strain and the decohesion strain. For a relatively rigid second phase, such as glass, the principal strain concentration in the polymer occurs in the regions between closely spaced particles (Fig. 4). Specifically, since nearly all of the strain is accommodated by the polymer, a uniaxial applied strain, ε_∞, is magnified in the region between the particles by:

$$\varepsilon/\varepsilon_\infty \simeq (1 - 2R/l)^{-1} \tag{4}$$

where l is the centre-to-centre spacing between particles and R is the sphere radius. For example, strain concentrations in the range 4 to 10 frequently occur in materials with a volume loading of ~ 0.3. Such strains are well into the non-linear deformation response regime of the matrix (Fig. 1) [4]. It seems reasonable, therefore, to regard debonding as a phenomenon that occurs primarily in regions between closely spaced particles and, furthermore, that appreciable permanent deformation of the intervening matrix occurs after debonding.

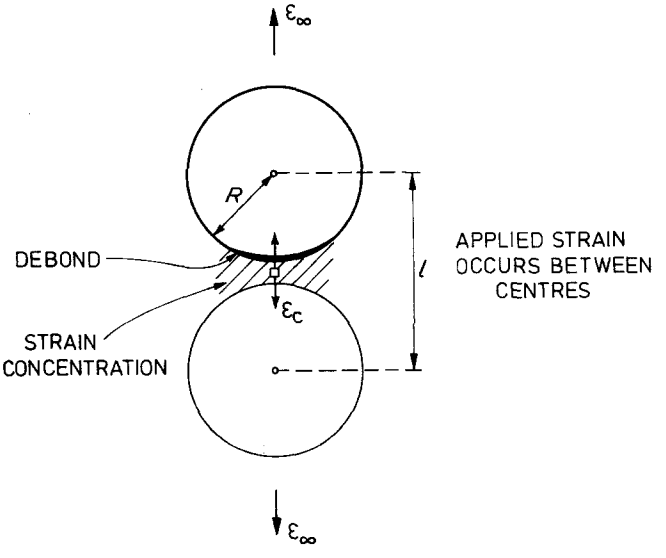

Figure 4 The strain concentration between closely spaced particulates and the associated interface debonding.

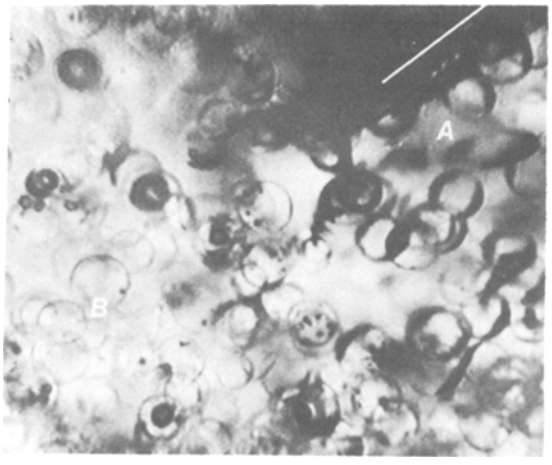

Figure 5 A micrograph illustrating debonding between closely spaced particulates in the crack tip process zone. The white lines outlines the crack. Regions A, B are the debonded and bonded zones, respectively [4].

Plastic deformation of the debonded matrix (analogous to plastic hole growth [7]) should result in permanent debonding and hence, the presence of residually debonded particles. A concomitant *dilatation* is expected in the process zone wake.

Experimental observations substantiate that debonding predominates in the region between particles [4] (Fig. 5). Furthermore, evidence of optical interference in the wake [4] is consistent with the presence of residual debonding. It is thus concluded that the non-linear loading features of the stress–strain curve (such as the tangent modulus) are dominated by matrix plasticity between debonded closely spaced particles; whereas the unloading (secant) modulus is governed by the elasticity of the composite containing debonded particles.

Micro-cracking or crazing of the matrix may constitute an alternative non-linear deformation mechanism. In this instance, the residual misfit strain due to differential shrinkage between the matrix and the particles results in residual tangential tensile stresses. Consequently, since the applied load imposes additional tangential tensile stresses, the potential for matrix microcracking between particles is readily visualized. Such microcracks would relieve the residual stress and be subject to residual opening [6]. Hence, non-linear behaviour accompanied by permanent dilatation and a reduced secant modulus would, again, be expected.

The observed stress–strain characteristics of particulate filled polymers are thus qualitatively explicable in terms either of enhanced plasticity of the matrix between debonded particles or of microcracking between particles. Specific distinction between these processes is not attempted in the subsequent analysis.

3. The fracture toughness

3.1. The energy density in the wake

The energy density and hence, the toughness, may be computed from the hysteresis in the stress–strain curve provided that an appropriate constitutive law can be specified. For simplicity, the loading curves pertinent to both the shear and dilatational deformation of the particulate filled polymers are assumed to exhibit a common form, suggested by the uniaxial stress, strain curve, i.e.

$$\sigma_{ij} = \sigma_y(\varepsilon_{ij})^n \tag{5}$$

where ε_{ij} is the inelastic strain, σ_y is the uniaxial yield strength, and n is a unique hardening coefficient. Unloading is assumed to be linear, with a secant modulus, E_s. With this idealization, many of the complexities of the toughening analysis [5–7] are eliminated, while still providing a useful perspective on trends in toughness with microstructure. The energy density based on Equation 5 has the form

$$\begin{aligned} U(y) &\equiv \oint \sigma_{ij}\,d\varepsilon_{ij} \\ &\approx \frac{\sigma_y}{(n+1)}\varepsilon_*^{n+1} - \frac{\sigma_y^2\varepsilon_*^{2n}}{2E_s} \\ &= \frac{\sigma_y\varepsilon_*^{n+1}}{(n+1)}\left[1 - \frac{\sigma_y\varepsilon_*^{n-1}(n+1)}{2E_s}\right] \end{aligned} \tag{6}$$

where ε_* is the maximum inelastic strain experienced by a material element within a strip, dy, distance y from the crack plane. The present choice of ε_* is predicated upon the non-linear solution for the principal strains in a crack tip field. For the present, idealized stress–strain law, the inelastic strains are [8, 9]:

$$\varepsilon_{ij} = \left[\frac{J}{I_n\sigma_y r}\right]^{1/(n+1)}\tilde{\varepsilon}_{ij}(\theta) \tag{7}$$

where r is the distance from the crack tip, $I_n \simeq 10(0.13 + n)^{1/2} - 4.8n$, and $\tilde{\varepsilon}(\theta)$ is the non-dimensional parameter given in [9]. Hence, the peak inelastic strain on the y plane becomes:

$$\varepsilon_* \simeq 2\left[\frac{J}{I_n \sigma_y y}\right]^{1/(n+1)} \quad (8)$$

The energy density is thus:

$$U(y) = \frac{2^{n+1}}{(n+1)}\frac{J}{I_n} \times \left[\frac{1}{y} - \frac{(n+1)}{2y}\left(\frac{\sigma_y}{E_s}\right)\left(\frac{J}{\sigma_y I_n y}\right)^{(n-1)/(n+1)}\right] \quad (9)$$

and the net energy in the wake is:

$$U \equiv \int_{r_0}^{h} U(y)\,dy = \frac{2^{n+1}}{n+1}\frac{J}{I_n} \times \left\{\ln\left(\frac{h}{r_0}\right) - \frac{(n+1)^2}{4}\left(\frac{\sigma_y}{E_s}\right)\left(\frac{J}{\sigma_y I_n}\right)^{(n-1)/(n+1)} \times \left[\frac{1}{r_0^{(n-1)/(n+1)}} - \frac{1}{h^{(n-1)/(n+1)}}\right]\right\} \quad (10)$$

where r_0 is the minimum distance from the crack plane at which the matrix between debonded particles experiences permanent deformation or microcracking. This distance should be of the order of the particle radius, because a crack typically deflects around one pole of the particle, leaving the deformed matrix at the opposite pole, in the wake. An upper bound energy (that neglects the recovery of elastic energy on unloading) is thus:

$$\hat{U} \simeq \frac{2^{n+1}}{(n+1)}\frac{J}{I_n}\ln\left(\frac{h}{R}\right) \quad (11)$$

The magnitude of J now requires further consideration. As evident from Equation 3, J varies within the zone from J_t to J_∞, due to the presence of the wake. However, since the deformation closest to the crack plane has the maximum influence on the net energy ($U(y) \to \infty$ as $y \to 0$, Equation 9), J_t is selected for present purposes.

3.2. Material degradation

The presence of debonding in the process zone degrades the local crack propagation resistance of the material, because cracks deflect into the debonded material at the poles of the particles. If debonding occurs at all particles immediately ahead of the crack tip, the area fraction of debonded material along the crack plane will be of the order of the volume fraction, f, of particles. Debonding represents a loss of section and hence, the simplest expression for the toughness degradation is [6]:

$$J_c^l = J_c^0(1-f) \quad (12)$$

where J_c^l is the degraded fracture resistance and J_c^0 is the reference fracture resistance of the matrix.

The degradation will not normally be as large as that determined by Equation 12 because some particles may not debond and a local toughening due to crack bowing [10] may then occur. Nevertheless, Equation 12 is used as the most convenient estimate for further analysis.

3.3. The toughness

3.3.1. Initial growth

The fracture toughness for initial growth of the crack, with a frontal process zone is simply obtained by equating J_t in Equation 1 to J_c^l in Equation 12 giving:

$$J_c^\infty \simeq J_c^0(1-f) \quad (13)$$

The toughness is thus predicted to be slightly reduced, due to the degradation of the material by debonding. However, as noted above, the degradation is not likely to be as substantial as that given by Equation 12. Hence, circumstances could be envisaged wherein the reduced near tip stresses (Equation 2), allow a small increase in toughness. Nevertheless, the effect should be small and, for all practical purposes, it is concluded that initial growth occurs at a toughness similar to that of the unreinforced matrix.

3.3.2. Steady state growth

When the crack has extended substantially into the debond process zone, the crack growth resistance approaches the steady-state solution. The upper bound toughness is deduced by obtaining J_∞ from Equations 3 and 11 and equating J_t to J_c^l (Equation 12) to give:

$$\hat{J}_c^\infty = J_c^0\left[1 - f + \frac{2^{n+2}}{(n+1)}\frac{\ln[h/R]}{I_n}\right] \quad (14)$$

Typically, for filled polymers the work hardening rate is low [3, 4], $n \simeq 0.2$. With this choice for n, the upper bound toughness becomes:

$$\hat{J}_c^\infty = J_c^0[1 - f + 0.8\ln(h/R)]. \quad (15)$$

where the zone width, h, can be approximately

related to the yield strength, via the plane strain relation [8]:

$$h \simeq \left[\frac{EJ_c^\infty}{\sigma_y^2}\right] g(n) \tag{16}$$

where $g \approx 1/4$ for $n = 0.2$.

A more complete solution for the steady state toughening can be obtained from Equation 10 as:

$$J_c^\infty = J_c^0 \left\{1 - f + \frac{2^{n+2}}{(n+1)I_n} \ln (h/R) - \frac{2^{n+1}}{4}(n+1)\frac{\sigma_y J_c^0}{I_n E_s}\left[\frac{J_c^0}{\sigma_y I_n R}\right]^{(n-1)/(n+1)}\right\} \tag{17a}$$

which for $n = 0.2$ becomes:

$$J_c^\infty = J_c^0 \left[1 - f + 0.8 \ln (h/R) - 0.06 \times \frac{\sigma_y J_c^0}{E_s}\left(\frac{J_c^0}{\sigma_y R}\right)^{2/3}\right] \tag{17b}$$

The specific dependence of J_c^∞ on h/R contained in the preceding formulas can be directly attributed to the selected form of the constitutive law (Equation 5). More realistic constitutive laws would undoubtedly yield a different functional dependence [5–7]. However, the general trends should be unaffected.

4. Comparison with experiment

Trends in the toughness with the volume fraction and size of particulates can be most expediently predicted using the upper bound formula (Equation 15), subject to the availability of independent determinations of the zone height, h. Such determinations have not been conducted, except in one instance [4] (Table I). In lieu of direct determinations of h, estimates may be obtained from Equation 16, provided that trends in modulus and yield strength are independently determined. Appropriate data are available for a glass filled epoxy (Table I). Note that, in the one instance for which h has been independently measured, the agreement with the value predicted from Equation 18 is relatively good. The toughness may be deduced from these data by combining Equations 15 and 16 to give:

$$J_c^\infty/J_c^0 = 1 - f + 0.8 \ln\left[\frac{EJ_c^\infty}{4\sigma_y^2 R}\right] \tag{18}$$

TABLE I Experimental data for glass sphere filled epoxy [4] ($y = 0.2\,\text{mm}\,\text{min}^{-1}$)

f	σ_y(MPa)	E(MPa)	J_{IC}(J m^2)	h(μm)
System I: $\langle R\rangle \approx 30\,\mu$m				
0.1	40	3.5	430	240
0.2	35	4.5	510	470
0.3	25	5.5	590	1290
System II: $\langle R\rangle \approx 13\,\mu$m				
0.1	40	3.5	550	300
0.2	35	4.5	690	630
0.3	25	5.5	900	2000

Measured h ($f = 0.25$, $\langle R\rangle = 30\,\mu$m) = 600 μm [4].

Before proceeding with the prediction, the choice of the reference toughness, J_c^0, must be consider. It is inappropriate to select the toughness of the unfilled polymer because, in the absence of particulates, alternative inelastic toughening mechanisms (e.g. craze growth) are activated. Predictions afforded by Equation 18 only pertain when the *same* inelastic process zone mechanisms operate. The application of Equation 18 must, therefore, be restricted to the prediction of trends in toughness *amongst* particulate-filled systems. Consequently, one particulate system is used as a reference and the relative behaviour of the other system is determined. The reference system selected is the material containing 10% (by volume) of the larger ($\langle R\rangle = 30\,\mu$m) glass spheres. The toughnesses relative to this system are predicted from Equation 18 and plotted in Fig. 6. A comparison with the measured toughnesses (Fig. 6) indicates good consistency for both particle radii. The approach thus appears to have merit and warrants further investigation.

5. Concluding remarks

A method of relating the toughness of a particulate filled polymer to an independently determined stress–strain curve for the composite has been demonstrated, using an idealized constitutive law. The analysis illustrates trends in particulate volume fraction and size and seems to predict behaviour consistent with measured trends.

Further understanding of particulate toughening based on the present concepts requires a superior characterization of the non-linear behaviour in the process zone, based on micromechanics models of the debonding,

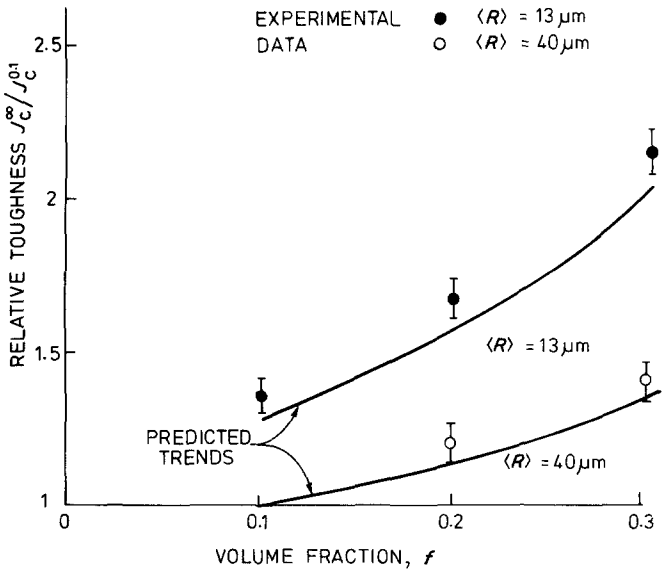

Figure 6 A comparison of trends in toughness predicted from the present analysis with experimental data. The toughness of the system with 10% of 40 μm radius spheres is taken as the reference.

microcracking and plasticity. More realistic constitutive laws can then be derived and used in a quantitative mode to predict trends in toughness. It would also be expedient to obtain direct measurements of the process zone width in the crack wake. Such determinations would constitute a superior measure of the utility of the present approach, as well as providing an independent assessment of the deformation characteristics within the process zone.

References

1. R. E. LAVENGOOD, L. NICOLAIS and M. NARKIO, *J. Appl. Polym. Sci.* **7** (1972) 1443.
2. J. C. MALLICK and L. J. BROUTMAN, *Mat. Sci. Eng.* **18** (1975) 63.
3. S. WILLIAMS, PhD thesis, University of Cambridge (1982).
4. A. B. OWEN, PhD thesis, University of Cambridge (1979).
5. B. BUDIANSKY, J. W. HUTCHINSON and J. LAMBROPOLOUS, *Int. J. Solids and Structures* **19** (1983) 337.
6. A. G. EVANS and K. T. FABER, *J. Amer. Ceram. Soc.* **67** (1984) 256.
7. A. G. EVANS, Z. AHMAD, D. G. GILBERT and P. W. R. BEAUMONT, *Acta Metall.* in press.
8. J. R. RICE and G. F. ROSENGREN, *J. Mech. Phys. Solids* **16** (1968) 1.
9. J. W. HUTCHINSON, *ibid.* **16** (1968) 13.
10. A. G. EVANS, *Phil. Mag.* **26** (1972) 1327.

Received 19 October
and accepted 22 November 1984